Review of Scientific Instruments

CO_2 laser heating system for *in situ* radial x-ray absorption at 16-BM-D at the Advanced Photon Source

Cite as: Rev. Sci. Instrum. **93**, 083901 (2022); https://doi.org/10.1063/5.0086642
Submitted: 27 January 2022 • Accepted: 02 July 2022 • Published Online: 05 August 2022

Christian Childs, Dean Smith, G. Alexander Smith, et al.

Review of Scientific Instruments | ARTICLE | scitation.org/journal/rsi

CO_2 laser heating system for *in situ* radial x-ray absorption at 16-BM-D at the Advanced Photon Source

Cite as: Rev. Sci. Instrum. **93**, 083901 (2022); doi: 10.1063/5.0086642
Submitted: 27 January 2022 • Accepted: 2 July 2022 •
Published Online: 5 August 2022

Christian Childs,[1,2,a)] Dean Smith,[3,4,a)] G. Alexander Smith,[3,5] Paul Ellison,[1] Daniel Sneed,[1,6] Jasmine Hinton,[1,3] Emily Siska,[3,5] Jeffrey S. Pigott,[7,b)] Eric Rod,[4] William O'Donnell,[1] Ran Salem,[8] Blake Sturtevant,[7] R. Jason Scharff,[9] Nenad Velisavljevic,[4,6] Changyong Park,[4] and Ashkan Salamat[1,3,a)]

AFFILIATIONS

[1] Department of Physics and Astronomy, University of Nevada Las Vegas, Las Vegas, Nevada 89154, USA
[2] Materials Science Division, Lawrence Livermore National Laboratory, Livermore, California 94550, USA
[3] Nevada Extreme Conditions Laboratory, University of Nevada, Las Vegas, Las Vegas, Nevada 89154, USA
[4] HPCAT, X-ray Science Division, Argonne National Laboratory, Lemont, Illinois 60439, USA
[5] Department of Chemistry and Biochemistry, University of Nevada Las Vegas, Las Vegas, Nevada 89154, USA
[6] Physics Division-Physical and Life Sciences Directorate, Lawrence Livermore National Laboratory, Livermore, California 94550, USA
[7] Shock and Detonation Physics (M-9), Los Alamos National Laboratory, Los Alamos, New Mexico 87545, USA
[8] Physics Department, Nuclear Research Center Negev, P.O. Box 9001, Beer-Sheva 84190, Israel
[9] Mission Support and Test Services, LLC, North Las Vegas, Nevada 89030, USA

[a)] **Authors to whom correspondence should be addressed:** christianmchilds10@gmail.com; dean.smith@unlv.edu; and ashkan.salamat@unlv.edu
[b)] **Current address:** School of Engineering, Case Western Reserve University, Cleveland, OH 44106, USA.

ABSTRACT

We present a portable CO_2 laser heating system for *in situ* x-ray absorption spectroscopy (XAS) studies at 16-BM-D (High Pressure Collaborative Access Team, Advanced Photon Source, Argonne National Laboratory). Back scattering optical measurements are made possible by the implementation of a Ge beamsplitter. Optical pyrometry is conducted in the near-infrared, and our temperature measurements are free of chromatic aberration due to the implementation of the peak-scaling method [A. Kavner and W. R. Panero, Phys. Earth Planet. Inter. **143–144**, 527–539 (2004) and A. Kavner and C. Nugent, Rev. Sci. Instrum. **79**, 024902 (2008)] and mode scrambling of the input signal. Laser power stabilization is established using electronic feedback, providing a steady power over second timescales [Childs *et al.*, Rev. Sci. Instrum. **91**, 103003 (2020)]—crucial for longer XAS collections. Examples of *in situ* high pressure–temperature extended x-ray absorption fine structure measurements of ZrO_2 are presented to demonstrate this new capability.

I. INTRODUCTION

The high brilliance of synchrotron sources and micro-focusing capabilities of x-ray beamlines enable x-ray absorption spectroscopy (XAS) measurements to be performed at high pressures in the diamond anvil cell (DAC).[4] X-ray absorption near edge structure (XANES) measurements allow the tracking of chemical environment, while extended x-ray absorption fine structure (EXAFS) measurements afford insight into local coordination and short-range ordering, each with element specificity, making them powerful

tools for investigating pressure-induced electronic[5] and structural[6] transitions including melting[7] and chemical reactions.[8,9]

Synchrotron beamlines dedicated to absorption spectroscopies at high pressure are becoming more commonplace,[10–12] and one such instrument is the 16-BM-D beamline of the High Pressure Collaborative Access Team (HPCAT; Sector 16, Advanced Photon Source, Argonne National Laboratory).[4] The bending magnet beamline has a typical flux of $\sim 5 \times 10^8$ photons/s at 30 keV and uses an energy-scanning monochromator for high energy-resolution in XAS measurements as well as micro-focusing for high spatial resolution (5×5 μm^2 FWHM) in XAS and x-ray diffraction (XRD) measurements.

XAS measurements at 16-BM-D are typically conducted in "radial" geometry, i.e., with x rays passing through a gasket of (semi-)transparent Be,[6] such that x-ray absorption lengths can be more easily matched, and "glitches" caused by diffraction from diamond can be easily avoided. Measurements may thus be made over distances of tens of micrometers, necessitating phase and chemical homogeneity over the entire width of the sample. Heating by a laser (LH-DAC) provides a controlled and localized method for annealing samples in DAC, sustaining high temperatures, and crucially does not heat the Be gasket material.

LH-DAC experiments commonly employ solid state near-infrared (NIR) lasers ($\lambda \sim 1$ μm) for direct absorption with metals and narrow-gap semiconductors.[13–16] However, the inverse-Bremsstrahlung absorption process[17] heats primarily the surface of materials, causing large temperature gradients and inhomogeneities, and is not compatible with wide bandgap materials. A common workaround for wide gap materials is the mixing of a metallic coupler with the sample, but this approach is incompatible with generating quality samples for XAS measurements. Alternatively, the use of CO_2 gas lasers, lasing in the mid-infrared, permits direct coupling with many insulating materials via anharmonic polariton-phonon scattering processes.[18–20]

We have recently studied local ordering in high-pressure phases of SnO_2[6] and Sn_3N_4[21] using EXAFS on samples generated by CO_2 laser heating.[20] In Sn_3N_4, a combination of EXAFS and XRD proved essential for distinguishing high-pressure phases with similar diffraction signatures, demonstrating the value of a dedicated CO_2 laser heating instrument at the combined diffraction and XAS beamline.

Here, we present a portable CO_2 laser heating instrument designed for compatibility with *in situ* XAS measurements at 16-BM-D. The present system features on-axis (i.e., normal to the diamond table) delivery of the CO_2 laser for simplified alignment, a stabilized CO_2 laser intensity,[3] reduced chromatic aberrations by design, and peak scaling temperature measurements producing two-dimensional thermal maps.[2]

This paper is organized as follows. In Sec. II, we discuss the underlying principles in the design of the system. In Sec. III, we describe the system layout in detail. A case study is presented in Sec. IV, showing EXAFS measurements of ZrO_2 at high pressure and high temperature.

II. DESIGN CONSIDERATIONS

A. Form factor

The sample position in 16-BM-D is dictated by the focused x-ray position, and the CO_2 laser spot must be brought to this position with micrometer precision. To preserve the alignment of the laser optical path while facilitating these movements, we designed a pre-aligned instrument that is placed on a three-axis translation stage inside the experimental hutch, such that the imaging microscope—co-aligned with the laser spot—can be aligned to the sample position. The large footprint of the CO_2 laser and the optical path length requirements were taken into account by designing a three-tier system of custom aluminum breadboards (Fig. 1), totaling $13 \times 29 \times 15$ in. ($330 \times 736 \times 381$ mm^3). Weight was relieved from each breadboard by removing material from the underside.

B. On-axis geometry

Previous CO_2 laser-heating instruments,[14] including our own,[20] have used an "off-axis" geometry wherein the laser radiation is introduced at some angle (on the order of 20°–30°) relative to the compression axis of the DAC. This geometry allows for "on-axis" (i.e., normal to the diamond table) viewing of the sample via secondary, visible-compatible optics, maintaining separate beam paths and optical devices for the mid-infrared laser light, and the visible image and thermal emission signal.

In large part, the motivation for maintaining separate optical paths for the CO_2 laser and imaging and analysis of the sample space is rooted in the challenging differences in material requirements—typical optical glasses absorb CO_2 laser light strongly. However, the alignment of the focused laser spot to the sample position in this geometry is complicated due to the refraction of the beam from the diamond ($n = 2.4$ at 10.6 μm), resulting in lengthy realignment procedures each time a new DAC is introduced. We have attempted to overcome these issues by imaging the direct primary beam with a mid-IR camera, with promising initial results,[20] but further development is required to refine this approach. The off-axis geometry also imposes constraints on compatible DAC designs—requiring an opening wide enough to facilitate the on-axis viewing as well as the off-axis focusing laser beam as well as on the choice of optics—the requirement for a separate laser-focusing and visible-imaging lens in close proximity means longer focal lengths for each, with implications for the minimum focused laser spot size, the imaging quality of the microscope component, and throughput of the optical pyrometer.

In practice, the off-axis geometry proves to be cumbersome when aligning the position of the focused CO_2 laser beam with the sample and x ray. Our present design thus uses an "on-axis" geometry—wherein the CO_2 laser light and all diagnostics are performed along the compression axis of the DAC (i.e., normal to the diamond table surface)—to alleviate issues from the more-complicated off-axis geometry and is a necessary step toward user-facing CO_2 laser heating instruments at a large-scale facility.[22] Additionally, since the XAS measurements at 16-BM-D are performed radially through the gasket of the DAC,[4] the optical axis is not impeded by x-ray instrumentation, allowing a lens to be placed in close proximity to the sample to maximize numerical aperture and improving laser focus as well as a light collection for spectral analysis and imaging.

The use of a single lens for heating and analysis requires a beam-splitting element to separate the mid-infrared laser light and visible/near-infrared information. For this, we identified Ge as an appropriate material. Ge is transparent at 10.6 μm and is routinely

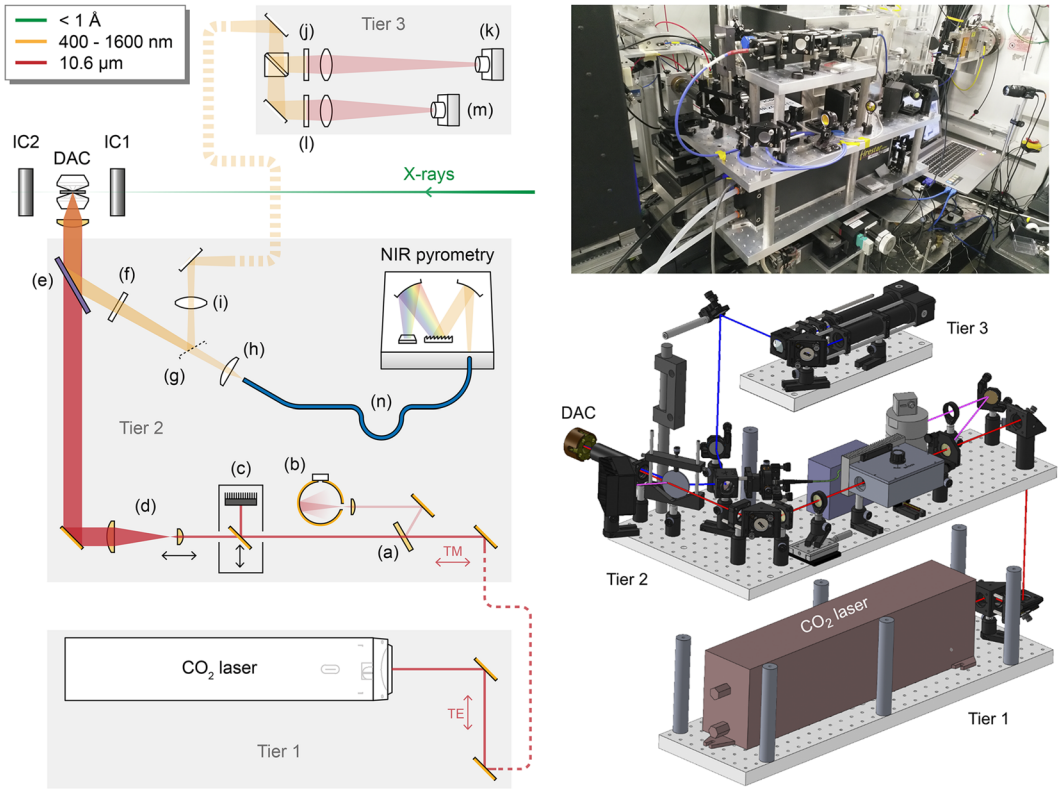

FIG. 1. (Left) Diagram of the optical layout of the CO_2 laser heating instrument, with components labeled: (a) a ZnSe AR-coated wedge window, (b) a 75 mm ZnSe lens focused into an integrating sphere and thermopile, (c) an electronic beam dump, (d) a beam expander, (e) a Ge window, (f) an MgF_2 window, (g) a 92:8 pellicle, (h) 16 mm aspheric lens and 1 mm fiber, (i) field lens, (j) 700 nm band pass and 150 mm biconvex lens, (k) peak scaling camera (Point Gray FL3-U3-32S2C), (l) 647 nm band pass and 100 mm biconvex lens, (m) visualization camera (WATEC LCL-211H), and (n) mode scrambler. (Top right) Photograph of the instrument in place at 16-BM-D. (Bottom right) Exploded CAD model showing three-tier construction of the CO_2 laser heating instrument.

used in mid-infrared optics while having good reflectivity in the visible (44% at 64° AOI, λ = 700 nm, unpolarized).

A lens that is compatible with the high-power 10.6 μm laser as well as visible light is required. ZnSe is highly transparent in the mid-infrared but has high absorption below around 600 nm and strong dispersion in the visible. We, therefore, use a 647 nm bandpass filter to avoid chromatic aberrations in our imaging optical path by selecting only a narrow wavelength range.

C. Peak-scaling method for temperature measurements

We opt for the peak-scaling method of measuring thermal emission to derive two-dimensional temperature maps, first proposed by Kavner, Nugent, and Rainey,[1,2,23,24] which has been successfully implemented in the LH-DAC.[25] The underlying principle of this method is to combine a spatially averaged thermal emission spectrum, collected from all locations in the heated sample, with a two-dimensional image of the heated sample collected at a nominal wavelength (here 700 nm). An iterative fitting procedure involving a simulated grey-body spectrum and the measured spatially averaged spectrum then converts pixel intensities from the image into temperatures. Thus, the microscope image gives information on the distribution of temperatures in the sample during heating. In the case of radial-geometry XAS measurements, where measurements are conducted across the entire length of the sample (typically tens of μm), such information is invaluable to ensure uniformity across the x-ray probe.

Peak-scaling differs from the widely used method of spatially resolved optical pyrometry, in which pinhole systems and optical magnification define a region of interest at the sample location that closely corresponds to the x-ray probe.[13,15,20] This spatially resolved approach is sensitive to chromatic aberrations, which negatively affect the accuracy of temperature derivations.[23,26–28] Instead, the peak scaling method captures thermal emission from the entire heated sample space into a spectrometer.

The dispersion of ZnSe is less pronounced in the near-infrared, and we, therefore, opt to collect thermal emission in the range of 1.0–1.6 μm. In doing so, we are able to ensure that the entire heated spot is imaged into a spectrometer with reduced chromatic aberration. Observing thermal emission in the near-infrared also provides greater sensitivity at lower temperatures as well as greater confidence in temperature derivations on materials whose emissivity does not favor significant emissions in the visible spectrum, i.e.,

visible-transparent materials relevant to CO_2 laser-heated studies, such as minerals or ceramics. A combination of monochromatic imaging and collection of the thermal spectrum in the near-infrared greatly reduces the chromatic aberrations in the system.

A MATLAB program was developed to perform the iterative fitting of two-dimensional images and the total thermal emission of the sample to generate two-dimensional temperature maps. Figure 2 shows two-dimensional maps of temperature across a 26 μm sample of ZrO_2. Both the average temperature T_{avg} and peak temperature T_{peak} are determined by a fitting of a sum of Planck profiles to the total thermal emission of the sample, with the number of Planck elements and their temperature distributions determined by the intensity at λ = 700 nm at each pixel within the defined region-of-interest [here 150 × 150 pixels; 100 × 100 μm^2, Figs. 2(a) and 2(b)]. The temperatures of each Planck element are then iterated to fit the spectrum from the entire hotspot [Fig. 2(c)]. Fitting temperature in this way allows insight into temperature distributions across the sample, which is crucial for XAS measurements that are taken radially through the entire width of the sample, where significant gradients could lead to structural or chemical inhomogeneities across the probe. In Fig. 2, the sample was heated to at least T_{avg} across its 26 μm width with minimal gradients, and Sec. IV shows the XAS data collected on the uniformly heated sample. The blue–green [Fig. 2(a)]/red [Fig. 2(b)] surrounding area is secondary heating of the NaCl encapsulating pellet (see Sec. IV for details on sample preparation).

III. OPTICAL LAYOUT

The optical layout comprises two parts: CO_2 laser delivery and visible/near-IR imaging and spectroscopy. The laser delivery is shown in the red paths in Fig. 1, while the diagnostics are shown in yellow.

A. CO_2 laser path

The Synrad Firestar *t*60 CO_2 laser sits on Tier 1 of the instrument. A system of two Au mirrors sends the laser light vertically, and a third Au mirror directs the light onto the optical plane of Tier 2. In doing so, the polarization of the light is converted from transverse electric (TE) at the laser source to transverse magnetic (TM) at the optical plane on Tier 2.

Direct modulation of the CO_2 laser power is implemented, stabilizing the laser power on the sample during XAS collections on the order of seconds or minutes.[3] A partial reflection <0.5% is picked off from the beam by a ZnSe wedged window (a) and directed into a custom-made integrating sphere (b) by an f = 75 mm ZnSe focusing lens. A thermopile sensor on integrating sphere (b) reads into a LabVIEW program, which varies the duty cycle of the current across the laser cavity to keep its power output constant. To prevent the large electrical noise from the laser controller from contaminating thermopile signals, an opto-isolator was added between the controller and the data acquisition device.

An enclosed, remote-controlled beam dump (c) was installed. The beam dump consists of an Au mirror on a motorized flip mount that is controlled remotely from outside the experimental hutch and directs the laser radiation into a graphite beam dump. This feature allows for the CO_2 laser beam to be switched on/off at the sample, without removing power from the tube, thus avoiding a necessary re-stabilization of the power.[3]

A variable Keplerian beam expander (d) expands the laser beam by ~ 2×. The beam expander (d) comprises a pair of ZnSe plano-convex lenses with f = 25 and 50 mm. The f = 25 mm lens may be translated along the beam path to control the collimation of the CO_2 laser beam between (d) and the ZnSe objective lens, thereby controlling the focal spot size at the sample position. Due to the large difference in the index of refraction of ZnSe in the mid-infrared and at our working wavelengths for imaging and spectral analysis, the beam expander (d) plays an important role in ensuring that the laser spot and diagnostics are confocal[29] as well as reducing the minimum spot size for the CO_2 laser.

After the beam expander (d), laser light is turned toward the DAC and objective axes by a final Au mirror. There, it is incident on a Ge window (e), which is used as a beam-splitting long-pass filter to separate mid-infrared and visible/near-infrared light in the

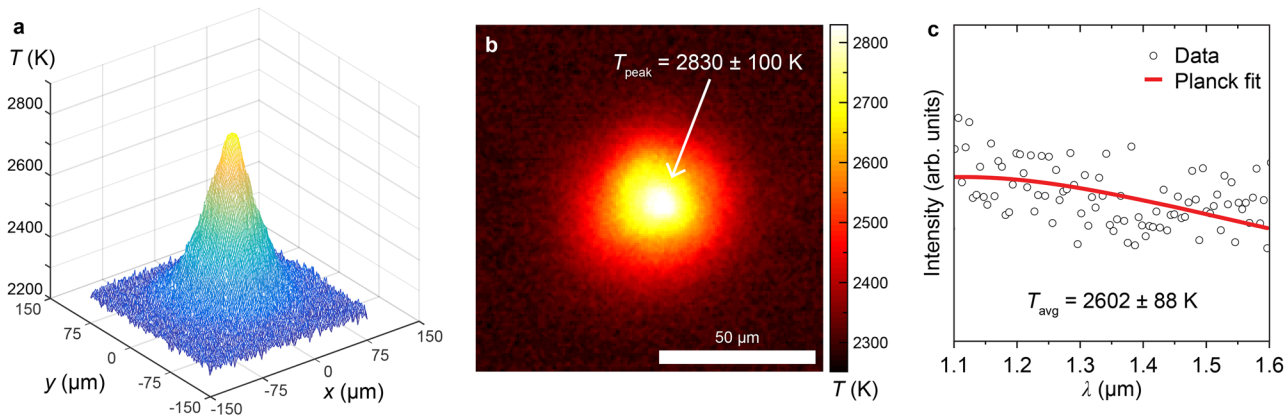

FIG. 2. (a) and (b) Map of temperature distributions across a sample of ZrO_2 heated with 50 W laser power, to a peak temperature T_{peak} of 2830 ± 100 K. The white and yellow regions in the center of (b) correspond to the ~26 μm ZrO_2 sample. (c) Representative one-dimensional thermal emission spectrum in the near-infrared, with results of Planck fit showing a T_{avg} of 2602 ± 88 K.

collection optics. The Ge window (e) is a 2 in. round with a thickness of 5 mm and is uncoated. Ge has an index of refraction of ~4 at 10.6 μm, leading to significant Fresnel reflections from both surfaces as the CO_2 laser beam passes through.[29] The initial conversion of the laser light into TM polarization by translating from Tier 1 to Tier 2 allows manipulation of the Fresnel reflections by altering the angle of incidence at the Ge window (e). In order to reduce these reflections, we have placed the Ge window (e) as close to the Brewster angle (~ 76° at 10.6 μm) as possible without reducing the clear aperture of the window beyond use. Placing the window at 64° gives a horizontal profile of 22.35 mm and reduces reflection losses to ~8% at each Ge surface—i.e., ~15% total loss. Future designs may benefit from a Ge window that is coated for lower reflections at 10.6 μm, but the effects of such a coating on visible and near-infrared reflections need also be considered.

Finally, the CO_2 laser light is focused into the DAC by an aspheric ZnSe (f = 25 mm at 10.6 μm) and placed 24 mm from the sample plane (~21 mm from the diamond table).

B. Optical collection path

The same ZnSe aspheric lens used to focus the CO_2 laser light is used to collect images and thermal emission signals from the heated sample.

The lens has an anti-reflective coating for 8–12 μm to reduce Fresnel reflections of the laser light but is highly reflective in the visible/near-IR, causing substantial glare in the image when axial lighting is included. Alignment of the instrument to the samples is, therefore, performed with rear illumination from a tungsten bulb. The AR coating also creates an interference pattern in recorded spectra, which must be taken into account by the spectral intensity transfer function.

The collected light is reflected by Ge window (e) toward the diagnostics branch of Tier 2. An MgF_2 window (f) is placed in the beam path to remove reflections of backscattered CO_2 laser light, preventing damage to glass optics. A pellicle beamsplitter (g) then transmits 92% of the collected light to a fiber-coupled spectrometer (Ocean Insight Flame NIR) and directs the remaining 8% toward imaging and peak-scaling cameras.

As discussed in Sec. II, optical pyrometry is performed in the 1000–1600 nm range. The thermal emission signal is focused on the entry of the fiber by an aspheric condenser lens with a nominal f = 16 mm (h). At these wavelengths, a spot with a geometric radius of <200 μm is produced at the plane of the fiber entry, with a ±100 μm field, equating to a ~400 μm image of the DAC region of interest at the fiber.

A fiber with a 1 mm core was selected; we found that smaller cores introduced a significant spatial dependence on the measured spectra due to the aberrated edges of the demagnified image not entering the fiber. The fiber was aligned longitudinally to the focus of the lens by visualizing the face of the fiber through the aspheric lens (h), and concentric alignment was confirmed by back-illuminating a 20 μm pinhole at the sample position such that an image of the pinhole was formed at the fiber entry.

Multimode fibers preserve the angular dependence of the input light. The recorded spectra of a spectrometer with a multimode fiber butt-coupled to its slit are thus dependent on the geometric conditions of the input light. By bending the fiber multiple times (n), the modes of the multimode fiber become scrambled and the resulting output is homogeneously averaged.

A 100 μm slit was installed on the Ocean Insight Flame NIR spectrometer for higher throughput, producing 13 nm spectral resolution. Calibration of the spectrometer and peak-scaling camera was performed using an assembly of a 50 μm pinhole placed in front of a calibrated bulb and cross-calibrated with a NIST traceable bulb on a separate optical system.

The ZnSe objective lens has f ~ 21 mm at 700 nm (the peak-scaling wavelength) and f ~ 20.5 mm at 647 nm (the imaging wavelength) and is placed 24 mm from the sample position. The light reflected toward the cameras thus forms an image ~50 mm after the pellicle beamsplitter (g) (~291.2 mm from the objective), at which a biconvex lens (i) with f = 175 mm is placed. The biconcave lens (i) acts as a field lens, reducing vignetting at the image plane of the cameras, which would complicate the peak-scaling analysis.

After the field lens (i), light is reflected by a pair of Ag mirrors to the plane of Tier 3. A 50:50 beamsplitter directs half of the light to the peak-scaling camera (Point Gray Flea 3, k), via a 700 nm bandpass filter (j) and an f = 150 mm biconvex lens, yielding a ~ 7× magnification of the image from the sample on the peak-scaling camera (k). The remaining light is directed to the visualization camera (m) via an Ag mirror, 647 nm bandpass filter (l), and f = 100 mm biconvex lens, yielding a ~ 5× magnification on the imaging camera (m).

IV. CASE STUDY: A HIGH TEMPERATURE–PRESSURE STUDY OF ZIRCONIA USING *IN SITU* X-RAY SPECTROSCOPY

We chose zirconia, ZrO_2, as a test case for the new instrument at 16-BM-D. ZrO_2 absorbs CO_2 laser light efficiently, has a rich phase diagram, an absorption edge that is compatible with studies at 16-BM-D,[4] and provides parity with our recent case study using a similar CO_2 laser-heating instrument.[20] Under ambient conditions, ZrO_2 takes its namesake baddeleyite structure ($P2_1/c$).[30–33] At high pressures and room temperature, baddeleyite transforms first into a distorted fluorite-like structure (*Pbca*, "ortho-I") at ~6 GPa,[34] and then into a cotunnite-type structure (*Pnma*, "ortho-II"), which persists until at least 1 Mbar.[35]

These types of XAS measurements at extreme conditions will permit the local coordination sphere of the metal absorbing atom to be directly probed, measuring coordination number, oxidation state, and specifically monitoring anion positions.

DACs of custom design were used and fitted with Be gaskets to permit measurements in radial geometry.[4] The absorption length of Zr at its K-edge (17 998 eV) was determined using the Elam database,[36] and full x-ray cross sections in the HEPHAESTUS software package[37] were calculated to 26 μm.

Dense pellets of ZrO_2 (99%, Alfa Aesar) with a thickness of ~15 μm were prepared by compressing powder in a DAC fitted with a stainless steel gasket. This thickness provides efficient absorption of the mid-infrared CO_2 laser radiation and far exceeds the $5 \times 5\ \mu m^2$ FHWM of the x-ray probe at 16-BM-D for optimized absorption measurements. Samples were then drawn from the dense pellets so that their length closely matched the absorption length.

A separate DAC was fitted with a stainless steel gasket that was pre-indented to a thickness of 25 μm and a circular chamber with a diameter of 150 μm in its center. This chamber was filled with

oven-dried NaCl powder, which was then compressed into a dense, optically transparent pellet. A cavity with dimensions similar to the ZrO_2 sample was made in the NaCl pellet, the sample inserted, a thin window of NaCl placed on top, and the entire assembly compressed. Using minimal laser power, the sample is then heated to confirm efficient absorption of the CO_2 laser light and sufficient thermal insulation from the diamonds by the NaCl.

Finally, the ZrO_2 sample in its NaCl encapsulation is removed from the steel gasket by laser micromachining,[38] and the encapsulated sample is placed in a DAC fitted with a Be gasket pre-indented to 30 μm and a 150 μm sample chamber in its center. The DAC was then gas loaded with Ar to a pressure of 2 kbar.[39] In this way, quasi-hydrostatic compression can be achieved on a sample that has 5 μm thermal insulation on either side and is confirmed to couple with the CO_2 laser.

XAS measurements were taken across the Zr *K*-edge centered at 17 998 eV, with a scanning range of 400 eV below the edge to 1000 eV above the edge, allowing optimum background subtraction and normalization of the XAS data. Each data point is an average of 5 scans, and the monochromator was swept through the energy range with varying resolution set to allow for the shortest time required for each scan while ensuring high enough spectral resolution for accurate analysis. This allowed for high-quality XAS data to be taken while the sample was continuously heated by the CO_2 laser.

Figure 3 shows XAS spectra of ZrO_2 before, during, and after CO_2 laser heating at 20 GPa to a peak temperature of 1300 ± 150 K. Prior to heating, the sample is in a mixed-phase state with contributions from both the ortho-I and ortho-II phases; heating has the effect of annealing the sample into the energetically favored ortho-II structure. This is evidenced most prominently in the shape of the absorption edge itself, which sharpens significantly [Fig. 3(a)] Similarly, the pre-edge feature around 17 985 eV becomes less intense but more clearly defined [Fig. 3(b)]. In the near-edge region, features around 18 040 and 18 070 eV disappear on heating. Each of these changes to the absorption spectrum is sustained once the temperature is quenched to 300 K by blocking the laser, which is consistent with annealing the sample into a stable phase.

Figure 4 shows the EXAFS spectra in momentum [Fig. 4(a)] and real [Fig. 4(b)] space during the same laser heating cycle. Higher *k* features become more resolved following the annealing, as we have previously described in cubic high-pressure SnO_2.[6] Perhaps,

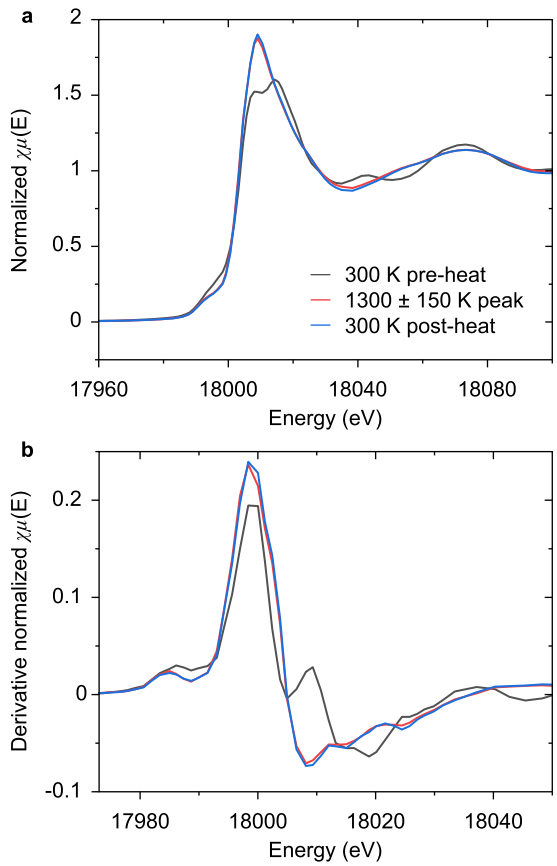

FIG. 3. X-ray absorption spectra of ZrO_2 at 20 GPa before (black), during, (red), and after (blue) laser heating to a peak temperature of 1300 ± 150 K. (a) A normalized absorption spectrum across the Zr *K* edge showing the XANES region and (b) an energy derivative of a normalized XAS spectrum.

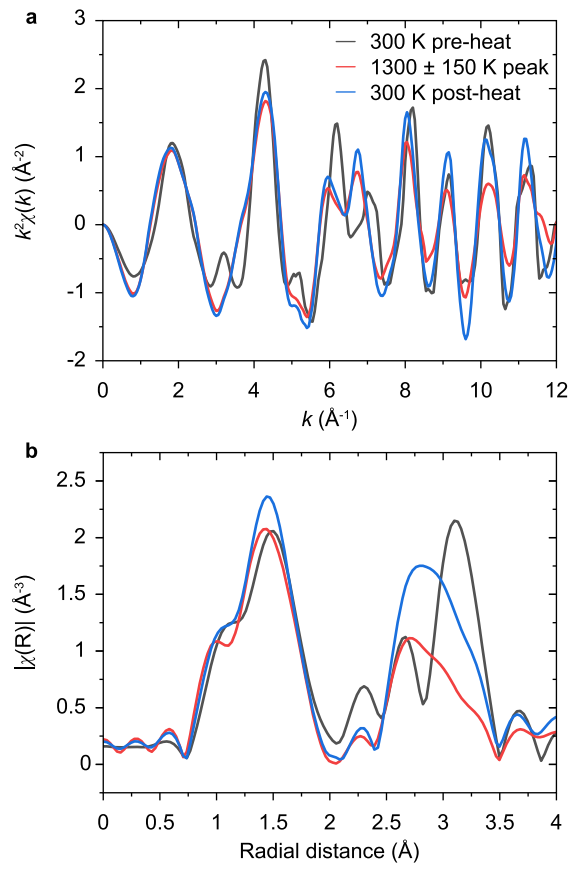

FIG. 4. EXAFS spectra of ZrO_2 at 20 GPa before (black), during (red), and after (blue) laser heating to a peak temperature of 1300 ± 150 K in (a) momentum space and (b) real space. Both are plotted with a k^2 weighting.

the most noteworthy difference is in the Zr–Zr and second Zr–O shells in the region of 2.5–3.4 Å, which show a significant difference following the thermal annealing to 1300 K. In particular, there is a shift in the strong Zr–Zr shell feature from 3.1 to 2.6 Å. This can be attributed to the rearrangement of Zr atoms from remnant *Pbca* (ortho-I) unit cells into the *Pnma* (ortho-II) structure, which is accompanied by a 0.5 Å reduction in Zr–Zr length.

V. CONCLUSIONS

We present a newly developed portable CO_2 laser heating system designed for use with XAS measurements in the diamond anvil cell at 16-BM-D of the Advanced Photon Source. Crucially, the implementation of a Ge window beamsplitter drastically simplifies the geometric requirements for such an instrument, which are typically hindered by the varying material requirements for visible and mid-infrared light. The present design has mid-infrared laser light and visible/near-infrared diagnostics by sharing a common objective lens that sits along the compression axis of the DAC, circumventing previous complications with alignment brought on by separate beam paths for laser and viewing optics. A promising further improvement is proposed by Spiekermann *et al.*[28] There, a near-infrared laser heating system is built very effectively around a parabolic reflector in place of a focusing lens, and the design in principle can be applied to CO_2 laser heating instruments to bypass the dependence on refractive optics made from ZnSe.

Temperature measurements use the peak-scaling method to generate two-dimensional temperature maps during heating. This allows inspection of the distribution of temperatures across the sample, an important consideration for XAS measurements that take place radially through the entire length of the sample.[4]

We demonstrate the efficacy of this instrument by performing high-pressure high-temperature experiments on ZrO_2 with *in situ* XAS measurements from which we are able to extract EXAFS data to 12 $Å^{-1}$ in momentum space and 4 Å in real space. At 1300 ± 150 K, we observe the thermal annealing of ZrO_2 across a sluggish phase transition from ortho-I to ortho-II, as shown by changes in the atomic distances derived by EXAFS.

ACKNOWLEDGMENTS

This work was supported, in part, by the National Nuclear Security Administration under the Stewardship Science Academic Alliances program through DOE Cooperative Agreement No. DE-NA0001982. Portions of this work were performed at HPCAT (Sector 16), Advanced Photon Source (APS), Argonne National Laboratory. HPCAT operations are supported by DOE-NNSA's Office of Experimental Sciences. The Advanced Photon Source is a U.S. Department of Energy (DOE), Office of Science User Facility, operated for the DOE Office of Science by Argonne National Laboratory under Contract No. DE-AC02-06CH11357. Portions of this work were performed under the auspices of Los Alamos National Laboratory. LANL is operated by Triad National Security, LLC, for the DOE-NNSA under Contract No. 89233218CNA000001. J.S.P. acknowledges support from the Harold Agnew National Security Postdoctoral Fellowship, with funding provided by LANL's Office of Experimental Sciences. This work was supported by Mission Support and Test Services LLC, under Contract No. DE-NA0003624 with the U.S. Department of Energy. Part of this work was performed under the auspices of the U.S. Department of Energy by Lawrence Livermore National Laboratory under Contract Nos. DE-AC52-07NA27344 and LLNL-JRNL-830581-DRAFT.

AUTHOR DECLARATIONS

Conflict of Interest

The authors have no conflicts to disclose.

Author Contributions

Christian Childs: Conceptualization (equal); Data curation (equal); Methodology (lead); Software (lead); Writing – original draft (equal). **Dean Smith:** Conceptualization (equal); Methodology (supporting); Writing – original draft (equal); Writing – review & editing (lead). **G. Alexander Smith:** Data curation (supporting); Formal analysis (supporting); Methodology (supporting). **Paul Ellison:** Methodology (equal); Resources (equal). **Daniel Sneed:** Data curation (equal); Formal analysis (lead). **Jasmine Hinton:** Data curation (supporting); Methodology (supporting). **Emily Siska:** Data curation (supporting). **Jeffrey S. Pigott:** Data curation (supporting); Investigation (equal); Resources (lead); Validation (equal). **Eric Rod:** Methodology (equal); Resources (equal). **William O'Donnell:** Methodology (equal); Resources (equal). **Ran Salem:** Methodology (supporting); Software (supporting). **Blake Sturtevant:** Project administration (supporting); Resources (supporting). **R. Jason Scharff:** Project administration (supporting); Resources (supporting). **Nenad Velisavljevic:** Project administration (supporting); Resources (supporting). **Changyong Park:** Conceptualization (supporting); Methodology (supporting); Resources (lead). **Ashkan Salamat:** Conceptualization (equal); Funding acquisition (lead); Methodology (supporting); Project administration (lead); Resources (lead); Supervision (lead); Writing – review & editing (supporting)

DATA AVAILABILITY

Raw data were generated at the Advanced Photon Source. The data that support the findings of this study are available from the corresponding authors upon reasonable request.

REFERENCES

[1] A. Kavner and W. R. Panero, "Temperature gradients and evaluation of thermoelastic properties in the synchrotron-based laser-heated diamond cell," Phys. Earth Planet. Inter. **143–144**, 527–539 (2004).

[2] A. Kavner and C. Nugent, "Precise measurements of radial temperature gradients in the laser-heated diamond anvil cell," Rev. Sci. Instrum. **79**, 024902 (2008).

[3] C. Childs, W. O'Donnell, P. B. Ellison, D. P. Shelton, and A. Salamat, "Optical and electronic solutions for power stabilization of CO_2 lasers," Rev. Sci. Instrum. **91**, 103003 (2020).

[4] C. Park, D. Popov, D. Ikuta, C. Lin, C. Kenney-Benson, E. Rod, A. Bommannavar, and G. Shen, "New developments in micro-X-ray diffraction and X-ray absorption spectroscopy for high-pressure research at 16-BM-D at the Advanced Photon Source," Rev. Sci. Instrum. **86**, 072205 (2015).

[5]D. Durkee, D. Smith, R. Torchio, S. Petitgirard, R. Briggs, I. Kantor, S. R. Evans, T. Chatterji, T. Irifune, S. Pascarelli, K. V. Lawler, A. Salamat, and S. A. J. Kimber, "Electronic origins of the giant volume collapse in the pyrite mineral MnS_2," J. Solid State Chem. **269**, 540–546 (2019).
[6]D. Sneed, J. S. C. Kearney, D. Smith, J. S. Smith, C. Park, and A. Salamat, "Probing disorder in high-pressure cubic tin (IV) oxide: A combined x-ray diffraction and absorption study," J. Synchrotron Radiat. **26**, 1245–1252 (2019).
[7]S. Boccato, R. Torchio, I. Kantor, G. Morard, S. Anzellini, R. Giampaoli, R. Briggs, A. Smareglia, T. Irifune, and S. Pascarelli, "The melting curve of nickel up to 100 GPa explored by XAS," J. Geophys. Res.: Solid Earth **122**, 9921–9930, https://doi.org/10.1002/2017jb014807 (2017).
[8]M. Muñoz, S. Pascarelli, G. Aquilanti, O. Narygina, A. Kurnosov, and L. Dubrovinsky, "Hyperspectral μ-XANES mapping in the diamond-anvil cell: Analytical procedure applied to the decomposition of (Mg, Fe)-ringwoodite at the upper/lower mantle boundary," High Pressure Res. **28**, 665–673 (2008).
[9]A. Dewaele, N. Worth, C. J. Pickard, R. J. Needs, S. Pascarelli, O. Mathon, M. Mezouar, and T. Irifune, "Synthesis and stability of xenon oxides Xe_2O_5 and Xe_3O_2 under pressure," Nat. Chem. **8**, 784–790 (2016).
[10]G. Aquilanti, O. Mathon, and S. Pascarelli, "Achievements in high-pressure science at the high-brilliance energy-dispersive x-ray absorption spectrometer of ESRF, ID24," J. Synchrotron Radiat. **16**, 699–706 (2009).
[11]O. Mathon, A. Beteva, J. Borrel, D. Bugnazet, S. Gatla, R. Hino, I. Kantor, T. Mairs, M. Munoz, S. Pasternak, F. Perrin, and S. Pascarelli, "The time-resolved and extreme conditions XAS (TEXAS) facility at the European Synchrotron Radiation Facility: The general-purpose EXAFS bending-magnet beamline BM23," J. Synchrotron Radiat. **22**, 1548–1554 (2015).
[12]L. Nataf, F. Baudelet, A. Polian, I. Jonane, A. Anspoks, A. Kuzmin, and T. Irifune, "Recent progress in high pressure x-ray absorption spectroscopy studies at the ODE beamline," High Pressure Res. **40**, 82–87 (2020).
[13]S. Petitgirard, A. Salamat, P. Beck, G. Weck, and P. Bouvier, "Strategies for *in situ* laser heating in the diamond anvil cell at an x-ray diffraction beamline," J. Synchrotron Radiat. **21**, 89–96 (2014).
[14]A. Salamat, R. A. Fischer, R. Briggs, M. I. McMahon, and S. Petitgirard, "*In situ* synchrotron X-ray diffraction in the laser-heated diamond anvil cell: Melting phenomena and synthesis of new materials," Coord. Chem. Rev. **277–278**, 15–30 (2014).
[15]Y. Meng, R. Hrubiak, E. Rod, R. Boehler, and G. Shen, "New developments in laser-heated diamond anvil cell with *in situ* synchrotron x-ray diffraction at High Pressure Collaborative Access Team," Rev. Sci. Instrum. **86**, 072201 (2015).
[16]S. Anzellini and S. Boccato, "A practical review of the laser-heated diamond anvil cell for university laboratories and synchrotron applications," Crystals **10**, 459 (2020).
[17]L. c. Ming and W. A. Bassett, "Laser heating in the diamond anvil press up to 2000 °C sustained and 3000 °C pulsed at pressures up to 260 kilobars," Rev. Sci. Instrum. **45**, 1115–1118 (1974).
[18]J. N. Hodgson, *Optical Absorption and Dispersion in Solids* (Springer, Boston, MA, 1971).
[19]P. M. A. Sherwood, *Vibrational Spectroscopy of Solids* (University Press, 1972).
[20]D. Smith, J. S. Smith, C. Childs, E. Rod, R. Hrubiak, G. Shen, and A. Salamat, "A CO_2 laser heating system for *in situ* high pressure-temperature experiments at HPCAT," Rev. Sci. Instrum. **89**, 083901 (2018).
[21]J. S. C. Kearney, M. Graužinytė, D. Smith, D. Sneed, C. Childs, J. Hinton, C. Park, J. S. Smith, E. Kim, S. D. S. Fitch, A. L. Hector, C. J. Pickard, J. A. Flores-Livas, and A. Salamat, "Pressure-tuneable visible-range band gap in the ionic spinel tin nitride," Angew. Chem., Int. Ed. **57**, 11623–11628 (2018).
[22]I. Kantor, C. Marini, O. Mathon, and S. Pascarelli, "A laser heating facility for energy-dispersive x-ray absorption spectroscopy," Rev. Sci. Instrum. **89**, 013111 (2018).
[23]L. R. Benedetti, N. Guignot, and D. L. Farber, "Achieving accuracy in spectroradiometric measurements of temperature in the laser-heated diamond anvil cell: Diamond is an optical component," J. Appl. Phys. **101**, 013109 (2007).
[24]E. S. G. Rainey and A. Kavner, "Peak scaling method to measure temperatures in the laser-heated diamond anvil cell and application to the thermal conductivity of MgO," J. Geophys. Res.: Solid Earth **119**, 8154–8170, https://doi.org/10.1002/2014jb011267 (2014).
[25]M. Kunz, J. Yan, E. Cornell, E. E. Domning, C. E. Yen, A. Doran, C. M. Beavers, A. Treger, Q. Williams, and A. A. MacDowell, "Implementation and application of the peak scaling method for temperature measurement in the laser heated diamond anvil cell," Rev. Sci. Instrum. **89**, 083903 (2018).
[26]M. J. Walter and K. T. Koga, "The effects of chromatic dispersion on temperature measurement in the laser-heated diamond anvil cell," Phys. Earth Planet. Inter. **143–144**, 541–558 (2004).
[27]L. R. Benedetti, D. L. Farber, and A. Kavner, "The great wedge: Quantifying chromatic aberration in imaging spectroscopy systems and application to temperature measurements in the laser-heated diamond anvil cell," J. Appl. Phys. **105**, 023517 (2009).
[28]G. Spiekermann, L. Libon, C. Albers, R. Sakrowski, S. Petitgirard, C. J. Sahle, M. Sundermann, H. Gretarsson, I. Sergueev, C. Sternemann, M. Wilke, and M. Murakami, "Reflective imaging, on-axis laser heating and radiospectrometry of samples in diamond anvil cells with a parabolic mirror," High Pressure Res. **41**, 142–154 (2021).
[29]M. Querry, "Optical Constants of Minerals and Other Materials from the Millimeter to the Ultraviolet," *US Army Armament Munitions Chemical Command Report No. ADA192210, 1987*; available at https://apps.dtic.mil/sti/citations/ADA192210.
[30]L.-G. Liu, "New high pressure phases of ZrO_2 and HfO_2," J. Phys. Chem. Solids **41**, 331–334 (1980).
[31]P. Bouvier, E. Djurado, G. Lucazeau, and T. Le Bihan, "High-pressure structural evolution of undoped tetragonal nanocrystalline zirconia," Phys. Rev. B **62**, 8731–8737 (2000).
[32]H. Öztürk and M. Durandurdu, "High-pressure phases of ZrO_2: An *ab initio* constant-pressure study," Phys. Rev. B **79**, 134111 (2009).
[33]A. Yoshiasa, H. Arima, K.-i. Murai, M. Okube, Y. Katayama, and O. Ohtaka, "High-pressure XAFS study of pure ZrO_2 and stabilized cubic ZrO_2," J. Phys. Soc. Jpn. **79**, 48–50 (2010).
[34]O. Ohtaka, T. Yamanaka, S. Kume, N. Hara, H. Asano, and F. Izumi, "Structural analysis of orthorhombic ZrO_2 by high resolution neutron powder diffraction," Proc. Jpn. Acad., Ser. B **66**, 193–196 (1990).
[35]O. Ohtaka, D. Andrault, P. Bouvier, E. Schultz, and M. Mezouar, "Phase relations and equation of state of ZrO_2 to 100 GPa," J. Appl. Crystallogr. **38**, 727–733 (2005).
[36]W. T. Elam, B. D. Ravel, and J. R. Sieber, "A new atomic database for x-ray spectroscopic calculations," Radiat. Phys. Chem. **63**, 121–128 (2002).
[37]B. Ravel and M. Newville, "ATHENA, ARTEMIS, HEPHAESTUS: Data analysis for X-ray absorption spectroscopy using IFEFFIT," J. Synchrotron Radiat. **12**, 537–541 (2005).
[38]R. Hrubiak, S. Sinogeikin, E. Rod, and G. Shen, "The laser micro-machining system for diamond anvil cell experiments and general precision machining applications at the High Pressure Collaborative Access Team," Rev. Sci. Instrum. **86**, 072202 (2015).
[39]D. Smith, D. P. Shelton, P. B. Ellison, and A. Salamat, "Simple imaging for the diamond anvil cell: Applications to hard-to-reach places," Rev. Sci. Instrum. **89**, 103902 (2018).